Additive Manufacturing 59 (2022) 103192

Contents lists available at ScienceDirect

Additive Manufacturing

journal homepage: www.elsevier.com/locate/addma

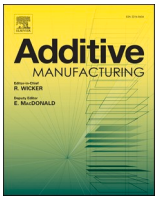

Design and validation of an innovative 3D printer containing a co-rotating twin screw extrusion unit

Joaquim Manoel Justino Netto [a,*,1], Amir Ilkiu Sarout [a], Andre Luiz Grando Santos [b], Alessandra de Almeida Lucas [b], Marcelo Aparecido Chinelatto [c], Jorge Lino Alves [d], António Gaspar-Cunha [e], José António Covas [e], Zilda de Castro Silveira [a]

[a] Department of Mechanical Engineering, São Carlos School of Engineering, University of São Paulo, Av. Trabalhador São-Carlense 400, 13566-590 São Carlos, Brazil
[b] DEMa, Federal University of São Carlos, Rod. Washington Luiz km 235, 13565-905 São Carlos, Brazil
[c] Department of Materials Engineering, São Carlos School of Engineering, University of São Paulo, Av. João Dagnone 1100, São Carlos, São Paulo 13563-120, Brazil
[d] FEUP, University of Porto, Rua Dr. Roberto Frias, 4200-465 Porto, Portugal
[e] DEP/Institute for Polymers and Composites, University of Minho, 4804-533 Guimarães, Portugal

ARTICLE INFO

Keywords:
Material extrusion additive manufacturing
Fused filament fabrication
Equipment design
Twin screw extruder

ABSTRACT

This paper presents the design and validation of an innovative 3D printer containing a co-rotating twin screw extrusion unit (Co-TSE). Single screw print heads were developed in the mid-2000s as an alternative to filament-based 3D printers, but they have limited process flexibility and mixing capacity. The new design accepts material in powder or micro-pellet form, and its dispersive and distributive mixing capacity can be fine tuned by setting output and screw rotation speed independently. The design combines a miniaturized modular Co-TSE operated under starve-fed conditions with a benchtop Cartesian platform. Numerical calculations were performed to ascertain whether the appropriate thermomechanical environment for polymer processing could be created by the proposed design. A prototype was built and extrusion tests were performed under different operating conditions, using polypropylene and a 90/10 wt% polypropylene/polystyrene blend. Two screw configurations were used, with and without kneading discs, to assess the response of the extrusion unit in terms of flow characteristics and mixing performance. The restriction to flow created by the mixing elements determines the starting melt position, and the average residence times, while their shearing and extensional action enhances homogenization effectiveness. The screw configuration and rotation speed do not affect the output, which depends only on the feed rate. Preliminary deposition tests were conducted to determine the feasible printing parameters. A standard tensile test specimen, a square scaffold and a multicolored rectangular box were successfully printed, validating the innovative design. The mechanical properties of printed test specimens were within the expected values.

1. Introduction

Stratasys' FDM® (fused deposition modeling) paramount patent was filed in 1989 [1]. This additive manufacturing technique consists in extruding a molten filament through a nozzle, which is then deposited as a series of consecutive X-Y planes (in the Z direction), in order to successively generate a 3D part. This disruptive technology revolutionized the toolbox of available manufacturing technologies, as it boosted rapid prototyping and opened the possibility of manufacturing complex parts without the need of a mold [2,3]. Apart from a few limitations that are inherent to the process, FDM requires material in filament form, i.e., the user is restricted to the relatively narrow available commercial offer. This generated efforts to develop material extrusion additive manufacturing technologies (MEX) accepting pellets or powders as raw material.

Polymer extrusion is a major industrial processing technology. While single screw extruders are generally adopted to yield continuous products with a constant cross-section (e.g., pipes and tubing, profiles, film & sheet, wire insulation, filaments and fibers), co-rotating twin screw extruders are increasingly used for compounding operations, i.e., polymerization, homogenization, devolatilization, additivation, blending, modification or polymer reinforcement, followed by pelletization [4].

* Corresponding author.
E-mail address: joaquim.netto@usp.br (J.M. Justino Netto).
[1] ORCID: 0000-0003-0251-4729.

https://doi.org/10.1016/j.addma.2022.103192
Received 20 June 2022; Received in revised form 28 September 2022; Accepted 30 September 2022
Available online 3 October 2022

These machines accept polymers in powder or pellet form and, depending on their geometrical features and operating conditions, can convey, melt, mix, devolatilize and generate pressure efficiently. Therefore, they are good candidates to be adopted in additive manufacturing.

Screw-assisted MEX additive manufacturing appeared in the mid-2000 s, typically adapting miniaturized vertical geometrically simplified single-screw extruders coupled to a positioning system, with a single heating zone and flood fed [5]. Since then, screw-assisted deposition tools have been further developed and find application in recycling [6, 7], biofabrication [8–12], low-cost metal and ceramic 3D printing [13–16], and personalized medicine [17–19]. Although single screw extruders offer an improved control over the plastication process and can reach higher deposition rates, their output is not solely dictated by the screw speed but also depends on nozzle geometry and polymer rheology. Moreover, their mixing ability is limited [20]. Recently, the development of desktop 3D printers with deposition tools based on miniaturized counter-rotating twin screw extruders (TSE) has been reported. Bhattacharyya et al. [21] designed a partially intermeshing counter-rotating TSE with variable pitch and shallow channels, to print multi-component bioinks in a single platform. A proof of concept prototype was built and tested to assess the mixing quality of a cell-loaded nanocomposite gel at ambient temperature, as well as the cell viability after deposition. Bai et al. [22] designed a fully intermeshing counter-rotating TSE, but a working prototype was not presented. It would be noted that counter-rotating TSE have good pressure generation capacity, but dispersive mixing is poor and the maximum attainable screw speeds must be very low in order to prevent premature screw and barrel wear [20].

Despite of their advantageous characteristics and increasing popularity for compounding operations and extrusion cooking, Co-TSE seem to have been largely ignored for additive manufacturing applications. This is probably due to the challenges involved in miniaturizing the complex screw geometry, as demonstrated in an earlier publication by the authors [23]. In the present study, the complete design of a Co-TSE AM system is presented and discussed. Numerical simulations are performed in order to assure that the hydrodynamic stresses, residence time and mixing developed by the small device are comparable to those of equivalent large scale machines. A prototype is built and tested in terms of plasticating performance and 3D printing feasibility. As in larger Co-TSE, the screws are modular, i.e., their profile can be adjusted to the characteristics of the polymer system being processed. A volumetric micro-feeder enables the independent setting of output and screw speed, which provides an opportunity to fine-tune dispersive and distributive mixing [24,25].

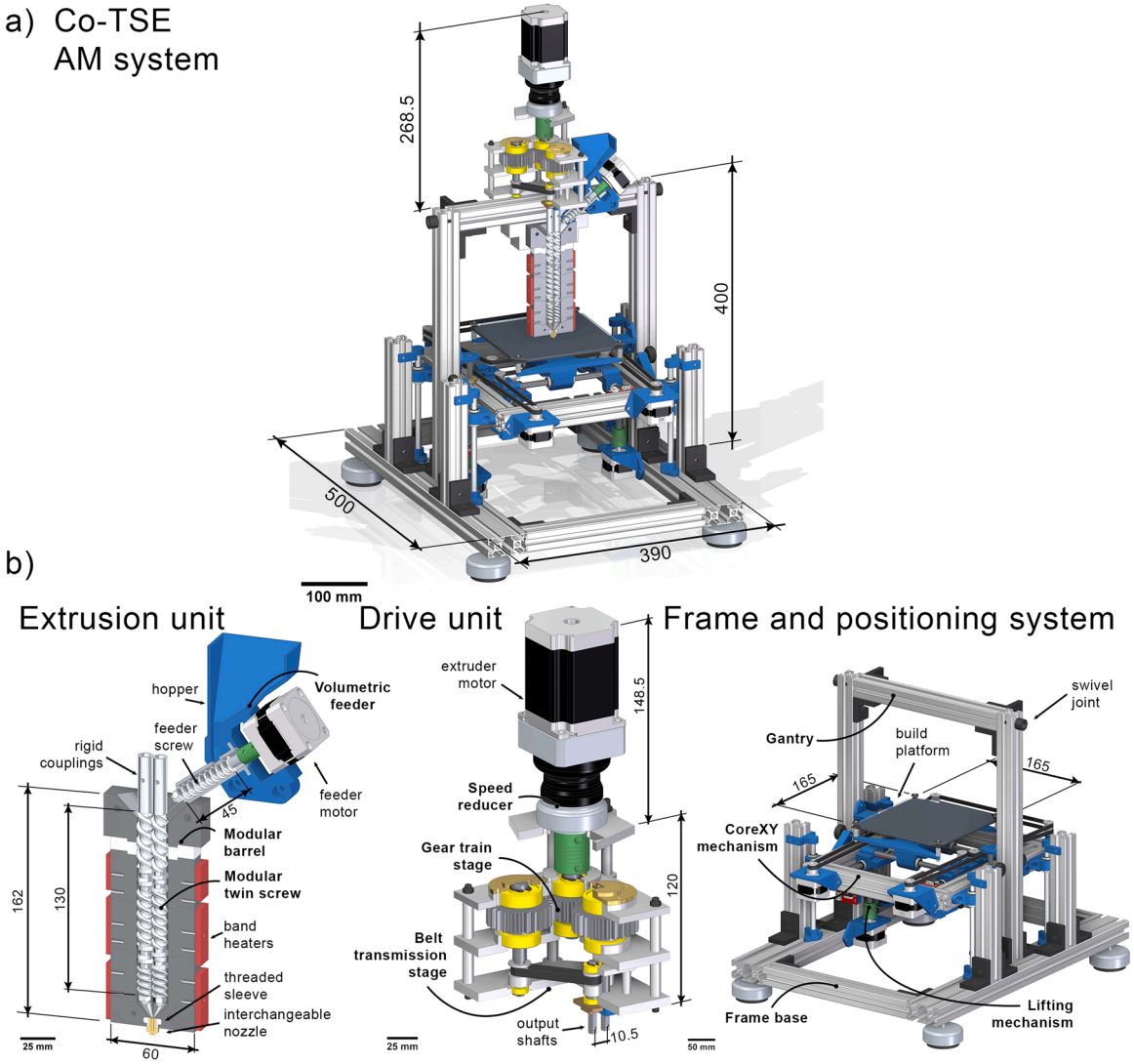

Fig. 1. The Co-TSE AM system: a) the complete 3D printer and b) its major subsystems.

2. Designing the prototype

Fig. 1 presents the Co-TSE AM system, which comprises three major subsystems: i) extrusion unit, ii) drive unit, and iii) frame and positioning system.

2.1. Extrusion unit

This unit comprises the (co-rotating) twin screws, barrel, band heaters, nozzle, and volumetric feeder. The screws (with a length/diameter (L/D) ratio of 11, an outer diameter of 12 mm and a maximum channel depth of 1.8 mm) are assembled from individual elements that are positioned axially along a hexagonal shaft (6 mm width across flats). These include conveying elements with various pitch/length combinations (20/40, 20/20, 15/40, 15/20, 10/35, 10/30, and 10/20) and 3 mm thick kneading discs that can be assembled to form kneading blocks. The former transport the material downstream at different rates, thus affecting the local residence times, degree of channel fill and heat transfer. The kneading discs may be staggered at positive or negative angle, thus inducing different levels of distributive/dispersive mixing, as well as residence times and viscous dissipation.

Rigid sleeves were specially designed to facilitate coupling with the drive unit, as well as to guarantee the correct relative positioning of the screws. The barrel is segmented to facilitate manufacturing and assembly. The segment upstream contains a feeding ramp that directs the material from the feeder into one screw. The bottom side is separated from the adjacent barrel segment by a polytetrafluoroethylene (PTFE) insulating barrier, in order to prevent premature polymer melting, whereas the top part allows fixing the barrel assembly to the structure. The maximum barrel capacity is 31 cm^3. The interchangeable extrusion nozzle is threaded to the barrel segment downstream. The volumetric feeder includes a 45 mm long screw (with a diameter 12 mm), a tubular barrel, a hopper with 75 cm^3 storage capacity and a Nema 17 stepper motor (model US17H4401, manufactured by Usongshine Inc., China).

2.2. Drive unit

One of the main challenges of designing a small Co-TSE is the short distance between the screw shafts (10.5 mm), which considerably limits the size of the driving components. In industrial Co-TSE machines, one screw shaft can be directly coupled to the motor, while two torsion shafts are used to drive the second screw. If the necessary torque is not achieved in a single reduction stage, two additional torsion shafts can be used on the first screw shaft [25]. Although the torsion shafts allow relatively small gears to withstand high torque levels, this technical solution would result in a complex and too large transmission system. In fact, any solution based solely on gear transmission seemed unfeasible due to the insufficient strength of the small teeth of at least one of the pinions. A specific gearbox composed of a simple gear train followed by a belt transmission stage was designed. In this way, power can be transmitted from a middle driving gear to two adjacent shafts, one of which is the first output screw shaft, and the other has an attached pulley to transmit power to the second output screw shaft. The gearbox is driven by a NEMA 23 stepper motor (model KTC-HT23–401, Kalatec Automation, Brazil) coupled to a planetary speed reducer (PEII 050–010, from Apex Dynamics Inc., USA), with a 10:1 N_{in}/N_{out} ratio, supporting a maximum torque of 18 N·m. The estimated torque available to each screw at different speeds (without considering transmission losses) is presented in Table 1.

2.3. Frame and positioning system

Since the print head is fixed to the gantry frame due to weight and inertia considerations, all movements are attributed to the build platform. A coreXY design is used for displacement in the X-Y plan, while the vertical motion is performed by two leadscrews. The vertical motion is guided by linear ball bearings and shafts positioned at the four corners of the coreXY frame. The coreXY mechanism allows the positioning system to be more compact and easily adjusted to the gantry structure. Four Nema 17 stepper motors (model US17H4401, Usongshine Inc., China) are used in the positioning system. The available print volume is 55 × 80×43 mm, enough for the intended benchtop applications of the Co-TSE AM system.

3. Process modeling

Due to design constraints and output considerations, the miniaturized Co-TSE has a length-to-diameter ratio (L/D), a screw rotation speed range, a feed rate, and available torque that are quite different from typical larger machines employed for polymer compounding operations. Therefore, before actually building the prototype, it seemed mandatory to ascertain whether the appropriate thermomechanical environment for polymer processing could be created by this design. For this purpose, the global plasticating modeling software for Co-TSE developed and validated by Teixeira et al. [4] was used to predict the axial evolution, from feeding to the die outlet, of the main process parameters, such as melt pressure, melt temperature, average shear rate, mechanical torque, local and cumulative residence times, and degree of fill.

As illustrated in Fig. 2, the screw configuration tested comprised two kneading blocks separated by conveying elements, which is typical for this type of extruder. The two mixing zones consisted of five kneading discs staggered − 60°, to promote melting (1st zone upstream) and dispersive mixing, respectively. 20/40, 15/40, and 10/20 conveying elements were used for the feeding zone, melt conveying, and pressure generation upstream of the nozzle. The feed rate (Q) was stipulated as 20 g/h (Q20) or 40 g/h (Q40), the barrel temperature (T_b) was set to 220 °C and the screw rotation speed to 80 rpm (N80) or 100 rpm (N100). The simulations assumed the extrusion of a generic grade of polypropylene (PP), whose main physical, thermal and rheological properties are listed in Table 2.

Fig. 2 depicts the evolution of (a) melt pressure and melt temperature, (b) average shear rate and cumulative torque per screw, (c) local and cumulative residence times, and (d) fill ratio along the screw axis at various operating conditions.

Polymer melting takes place through a combination of heat transfer and mechanical dissipation. The presence of restrictive kneading elements causes the screws to work fully filled immediately upstream, which facilitates these mechanisms. Thus, it is clear from Fig. 2a that the material melts just before attaining the first kneading block. The initial temperature increase is sharper than that observed in practice, as it is a consequence of the melting mechanism implemented in the overall plasticating model. The melt temperature tends to increase due to viscous dissipation associated with shearing. As expected, higher shear rates are produced at higher screw speeds. The shear rate is about two times higher in fully filled regions. Therefore, the melt temperature increase is more pronounced at the end of the intermediary conveying element. In addition, changes in the shape of the velocity profile cause the maximum shear rates to decrease when the feed rate increases [4]. That is why the melt temperature can reach 268 °C (for a set value of 220 °C) for the highest screw speed and lowest feed rate. Despite the

Table 1
Estimated torque available to each screw at different screw speeds.

Screw rotation speed (rpm)	10	20	30	40	50	60	70	80	90	100
Torque per screw (N m)	9.0	7.5	6.5	4.5	4.0	3.5	3.5	2.5	1.5	1.0

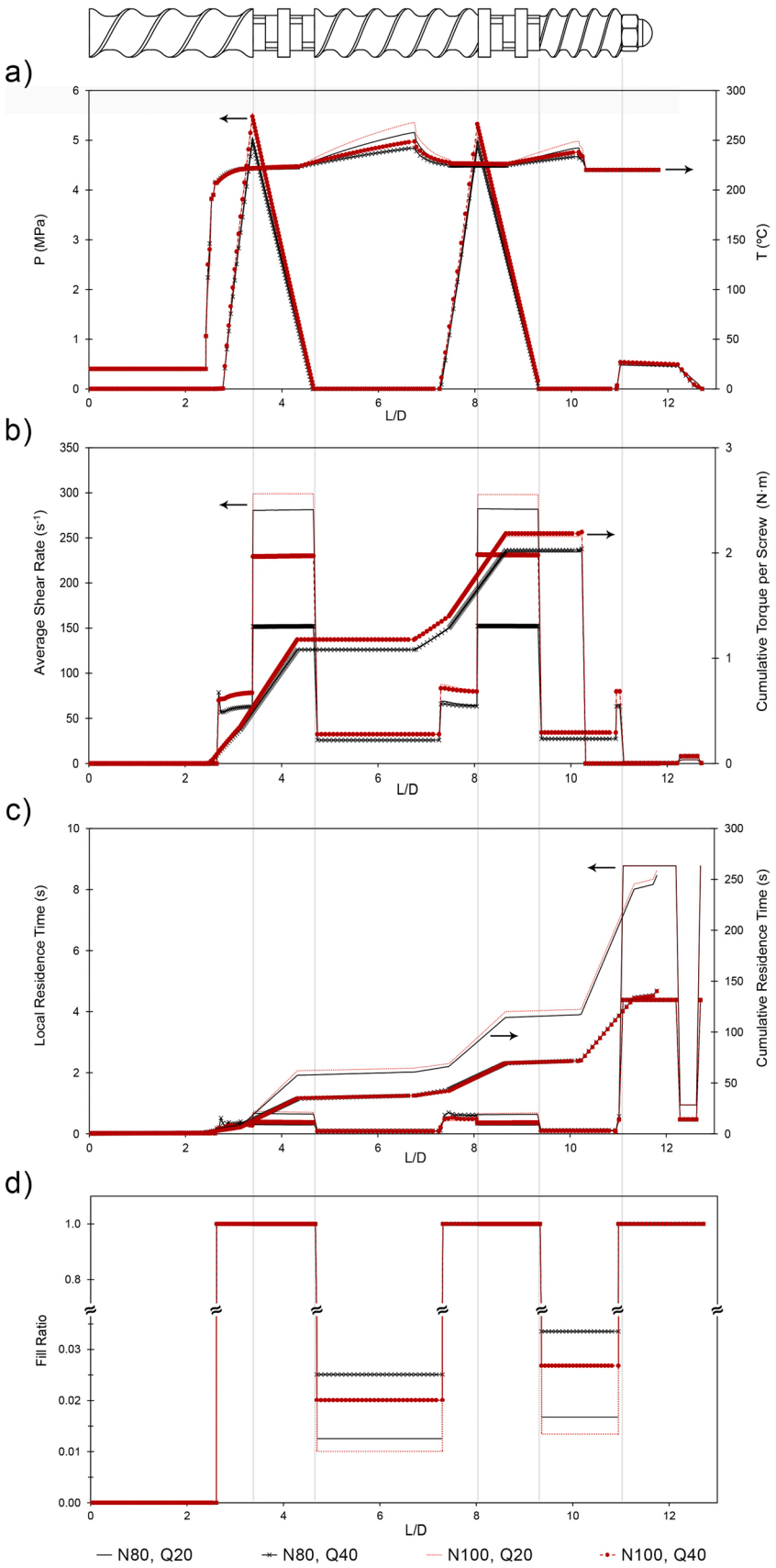

Fig. 2. Evolution of a) melt pressure and melt temperature, b) average shear rate and cumulative torque per screw, c) local residence time and cumulative residence time, and d) fill ratio along the screw axis under different operating conditions.

Table 2
Properties of the generic polypropylene grade used.

Property			Value	Unit
Density	Solids	ρ_s	560	kg m^{-3}
	Melt	ρ_m	740	
Thermal Conductivity	Solids	k_s	0.1	W m^{-1} °C^{-1}
	Melt	k_m	0.16	
Specific Heat	Solids	C_s	2480	J kg^{-1}
	Melt	C_m	2950	
Melting	Heat	H	60×10^3	J kg^{-1}
	Temperature	T_m	170	°C
Viscosity (Carreau-Yasuda law)		η_0	3500	Pa s
		E/R	7500	K
		λ	0.11	s
		a	0.97	
		n	0.33	
		T_0	260	°C

temperature-dependent melt viscosity, the pressure peaks tend to increase at higher screw speeds due to the increased rate at which material is conveyed backward in the kneading blocks. The effect of the feed rate on the pressure is less marked due to the non-Newtonian character of the melt. The maximum pressures are developed upstream of the kneading blocks, and can reach 5.5 MPa when the screws rotate at 100 rpm. As expected, between the two kneading blocks, the screws work mostly partially filled, and the pressure in these regions is nil. Obviously, flow through the nozzle requires pressure generation upstream, but the value of about 1 MPa depends much less on the feed rate.

Fig. 2b confirms that the shear rates in conveying zones are much lower than those in kneading blocks, not only because in the first case flow develops mostly in partially filled channels (with exception of a few downstream screw turns) but also due to the restrictive nature of the kneading elements. As their conveying capacity is limited, the melt is forced through very narrow gaps between the discs. As discussed before, shear increases with increasing screw speeds, but decreases with increasing feed rates. The shear rates range from about 150–300 s^{-1}, matching well the range of rates created in a larger Co-TSE [4]. The figure also demonstrates the crucial importance of the restrictive zones to the overall required torque (the value attaining 2.2 N·m with the screws at 100 rpm). The behavior of the cumulative torque follows the same trends as the pressure.

Obviously, the higher the feed rate and the higher the screw speed, the lower the residence time (Fig. 2c). Again, the contribution of restrictive zones to this parameter is paramount. The results show that doubling the output leads to a decrease in the residence time of about 45 %. In turn, the effect of the screw speed is much less pronounced due to the proximity of the values simulated. Besides the feed rate and screw speed, the residence times are related to the extruder L/D. Typical Co-TSE have L/D ranging from 30 to 40:1, and operate at accordingly much higher feed rates and screw speeds. Considering the proposed L/D ratio and the operating conditions, the cumulative residence times range from 140 to 260 s, which fall within the range observed in larger extruders.

As shown in Fig. 2d, the screws work fully filled (fill ratio of 1) in restrictive sections (where pressure and average shear rate rise), while the fill ratio is actually low in the conveying sections within the experimental range of outputs and screw speeds utilized. This promotes local distributive mixing and short residence times.

4. Prototype building

The screw elements were made by selective laser melting (SLM) in an MLab 200R machine (Concept Laser GmbH, Germany), using a cobalt-chromium-tungsten alloy. The rigid coupling sleeves were made by direct metal laser sintering (DMLS) in an EOSINT M280 machine (EOS GmbH, Germany) using maraging steel. The 3D printed parts were made with excellent geometric fidelity in a very short time. However, the resulting surface roughness was inappropriate for use and further polishing was mandatory. Fig. 3 displays the various fabrication stages of the twin screws.

The remaining components of the print head were obtained by conventional machining processes. The main frame and positioning system were put together from commercially available parts, with some specific components obtained by fused filament fabrication. The gantry has a manual swivel mechanism to position the print head assembly in the horizontal, facilitating screw and barrel removal. Fig. 4 shows the final Co-TSE AM system, evidencing the use of the swivel mechanism for maintenance.

Fig. 5 presents the electrical circuits used to control the equipment. The drive unit and volumetric feeder (Fig. 5a) are controlled by an Arduino Uno (Arduino, Massachusetts, USA). The driver WD-2404 (Wotiom, São Paulo, Brazil) is used for the Nema 23 motor, which operates in 1/16 microstepping mode. The driver DRV8825 (Pololu, Nevada, USA) is used for the Nema 17 motor, operating in 1/2 microstepping mode. The motors speed can be set individually with the Arduino IDE. Fig. 5b shows the circuit used to control the positioning system and the temperature of the build platform and extruder heaters. The setup consists of a typical RepRap Arduino Mega Pololu Shield (RAMPS 1.4), which was adapted to the project. The first heating zone of the extruder (close to the feeding zone) uses a pair of 60 W power band heaters associated to thermistor T2. The second heating zone uses two pairs of 100 W heaters, associated to thermistor T1. Thermistor T0 is used to control the heated build platform. A modified version of the Marlin firmware was loaded to the RAMPS, so that G-code commands generated by a commercial slicing program (e.g. Repetier-Host) could be used to control the position and temperature of the build platform as well as the temperature of the heating zones.

5. Experimental validation

Before testing the equipment, the volumetric feeder must be calibrated with the material used. Polypropylene copolymer (grade RP141 manufactured by Braskem, Brazil, for injection molding applications), was ground in a Mikro Bantam hammer mill (Hosokawa Micron Powder Systems, USA) after immersion in liquid nitrogen, to yield powder with particle size ranging from 300 to 600 μm. Fig. 6 shows the linear correlation obtained between feed rate (g/h) and the feeder screw speed (rpm).

5.1. Extrusion tests

The key characteristics of the new Co-TSE were investigated using the screw geometry simulated in Section 3 (configuration 1), and an alternative conveying screw without kneading discs (configuration 2), see Table 3. The temperatures of the first and second heating zones were set to 180 °C and 210 °C, respectively. The tests were performed with a 0.6 mm diameter brass 3D printing nozzle.

The capacity to set output and screw speed independently and operate under steady state was demonstrated simply by weighing the extruded material collected at one minute intervals, at different processing conditions (screws rotating at 40 rpm and 80 rpm, feed rates of 20 g/h and 40 g/h). Based on the numerical calculations for screw 1, the maximum screw speed tested was 80 rpm to avoid stalling due to insufficient torque at 100 rpm. The feed rates were stipulated so that the average shear rate at the kneading blocks could reach at least 100 s^{-1}. The linear relationships depicted in Fig. 7 and the virtual overlapping of the graphs for the two screw configurations demonstrate the validity of the assumption.

Fig. 8 shows the results of pull-out experiments performed with the two screw configurations. They consisted in interrupting steady state extrusion by stopping the feeder and screw rotation and removing the barrel as quickly as possible. As seen in Fig. 8a, solid particles survived only up to the start of the kneading zone upstream, as predicted

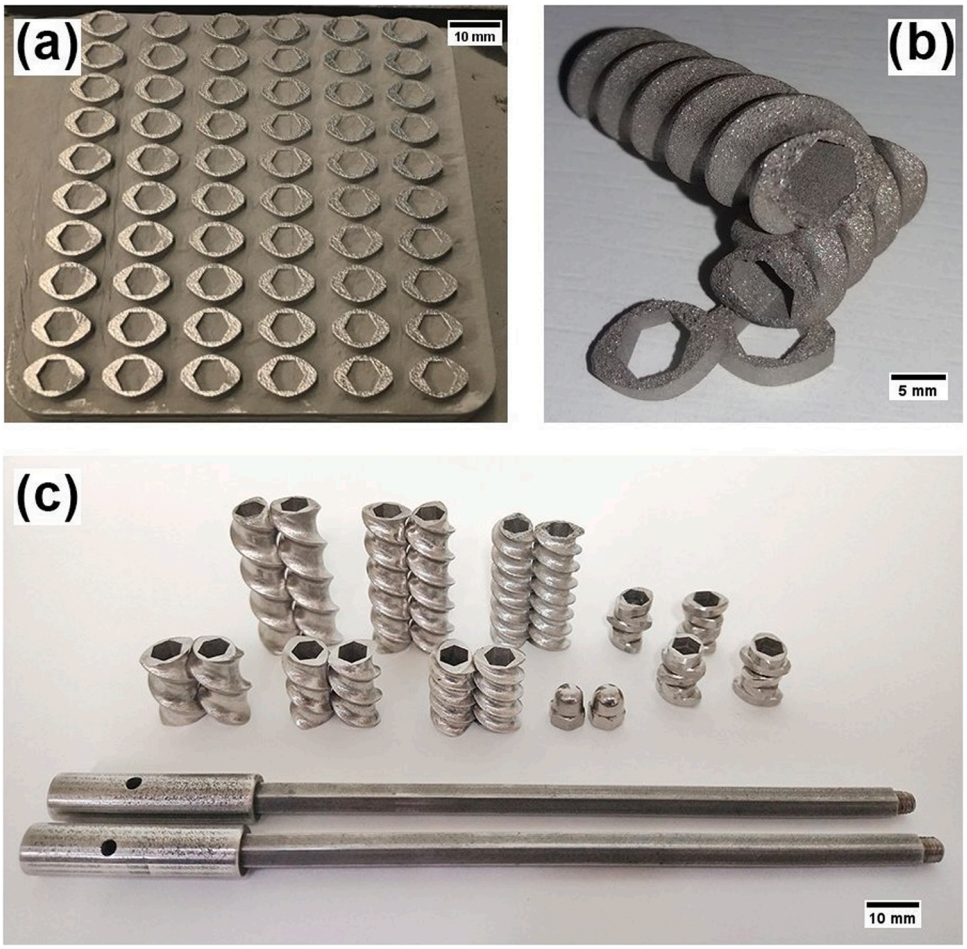

Fig. 3. Fabrication stages of the twin screws: (a) kneading discs obtained by SLM, (b) detail of the as-printed elements showing the poor surface finish, (c) set of screw elements and screw shafts coupled to the 3D printed sleeves after post-processing.

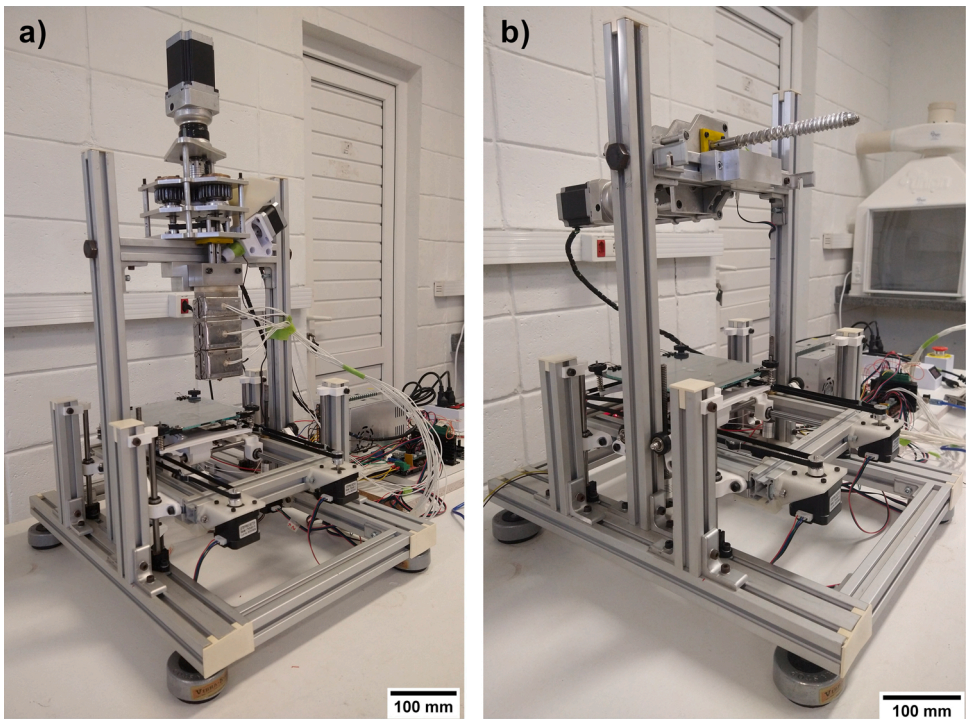

Fig. 4. The Co-TSE AM system: (a) operation position and (b) maintenance position, without the barrel and heaters.

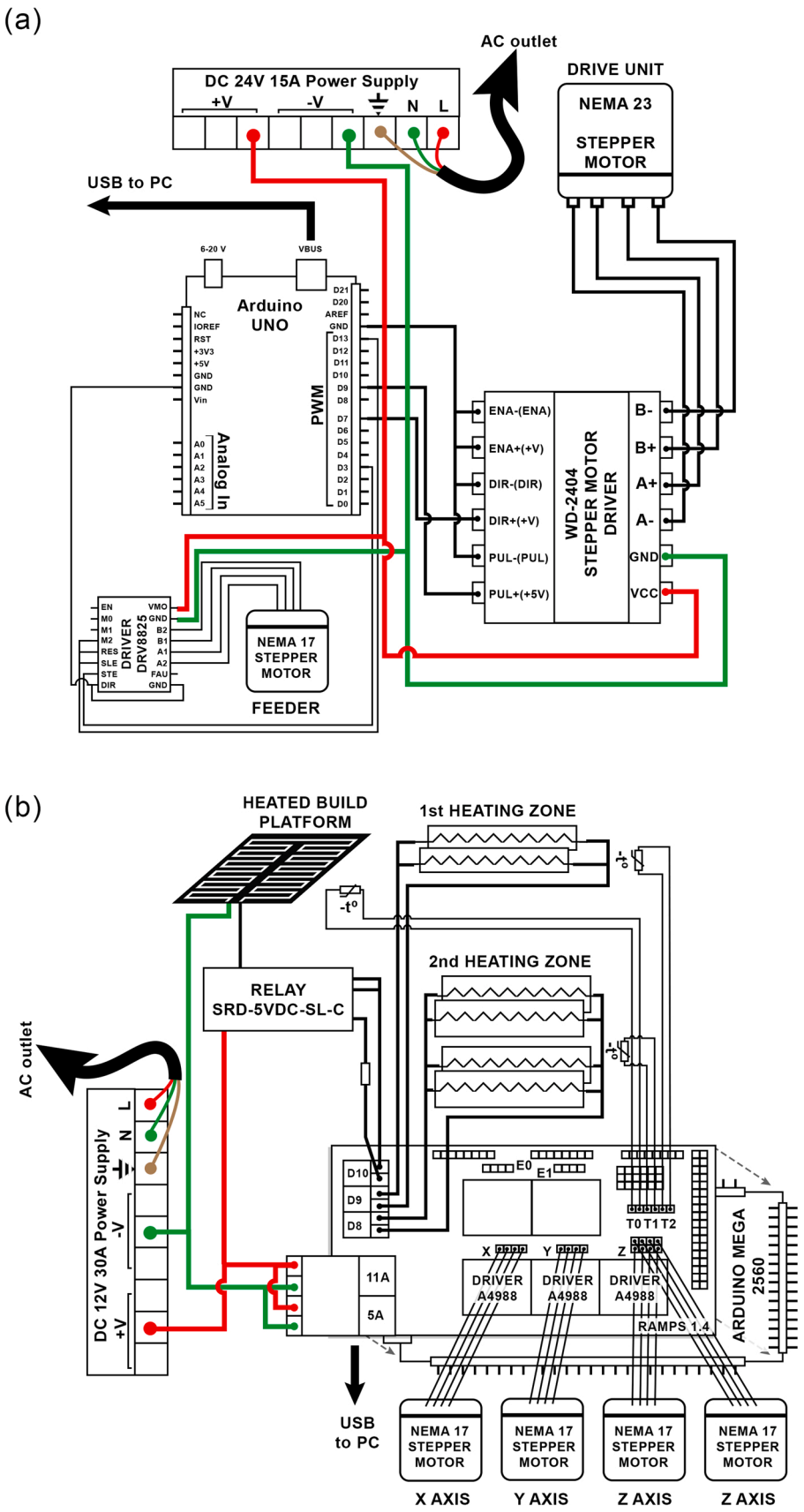

Fig. 5. Electrical circuits used to control (a) the drive unit and feeder, and (b) the position and temperature of the build platform and of the temperature of the extruder heating zones.

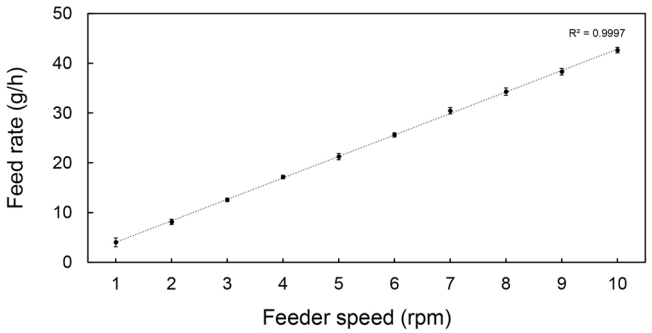

Fig. 6. Feed rate versus feeder speed for the PP micro-pellets.

Table 3
Screw configurations tested.

Screw configuration	Element				
1	20/40	KB-60/5/15*	15/40	KB-60/5/15*	10/20
2	20/40	15/40	10/30	10/20	

*The kneading blocks (KB) are identified as stagger angle/number of discs/total length.

numerically in Section 2. As the restriction to flow created by the discs forced the screw channels to become fully filled, heat transfer became more efficient, promoting melting. In the case of configuration 2, i.e., in the absence of kneading discs (Fig. 8b), the degree of screw filling increased progressively downstream due to the geometry of the conveying elements. When the screw finally became fully filled, melting took place, but much later than for configuration 1. The figure also shows that the screw length available for mixing the molten material before flow through the nozzle is much higher for configuration 1 (and will be further promoted by the presence of a second kneading zone).

The cumulative residence times were estimated by feeding a small amount of a red tracer directly to the co-rotating screws during steady state extrusion, and measuring the time elapsed until a color change could be visually detected in the extrudate. In fact, this procedure identifies the minimum residence time. However, given the typical shape of residence time distribution curves for Co-TSE, the values obtained should not be too different from average residence times [26]. As expected, the experimental residence times for screw configuration 1 are higher than for the non-restrictive configuration 2 for all processing conditions. Although a direct comparison with the numerical predictions made in Section 2 cannot be made as different residence times are involved, Table 4 shows the same dependency of residence time on the operating conditions for screw configuration 1.

The dispersive mixing capacity of the extruder and its dependence on the operating conditions were investigated by processing an immiscible blend of polypropylene and polystyrene (PS). The same PP used above was pre-mixed with 10 wt% of PS N1921 (Innova, Brazil), and fed to the extruder at 20 g/h using screw configurations 1 and 2. Samples of the extruded filaments along their length were collected and fractured after immersion in liquid nitrogen. The fractured surface of the samples was etched in acetone at room temperature for 3 h to remove the PS phase. The samples were sputter coated with gold and subjected to scanning electron microscopy (SEM) analysis, using a Leo 440 instrument (Zeiss, Germany). Fig. 9 shows the morphologies observed by SEM, where the dark holes and circular contours correspond to the PS domains that were dispersed in the PP matrix.

The size of the PS droplets was analysed using the software Image J. The analysis was made with 4–5 SEM images for each processing condition, allowing to identify at least 500 particles per treatment. The diameter of each droplet (d_i) was calculated from the corresponding area identified by the software and registered in histograms. The number-average diameter (d_n), volume-average diameter (d_v), and polydispersity (P) were calculated as [27]:

$$d_n = \frac{\sum_{i=1}^{N} n_i \times d_i}{\sum_{i=1}^{N} n_i} \quad (1)$$

$$d_v = \frac{\sum_{i=1}^{N} n_i \times d_i^4}{\sum_{i=1}^{N} n_i \times d_i^3} \quad (2)$$

$$P = \frac{d_v}{d_n} \quad (3)$$

The resulting histograms of PS droplet diameter distribution together with the calculated d_n, d_v and P are shown in Fig. 10. For screw configuration 1, it is clear from Fig. 10a and b that increasing the screw speed from 40 to 80 rpm caused a general reduction of the droplet diameter and a narrower size distribution, evidencing the improved dispersive mixing that can be achieved with the kneading discs. Screw configuration 2 produced a size distribution only marginally coarser than that observed for configuration 1 at 40 rpm, but there was no improvement with increasing screw speed.

Finer dispersion was achieved with configuration 1 at 80 rpm due to the capacity of the downstream kneading element to force the melt through the gap between the edge of the discs and the barrel wall. The negative staggering angle increases such effect as material recirculates around the discs. The kneading blocks create intense shear and elongational flows, the latter being particularly effective in breaking liquid droplets [20,25]. It is worth noting that, since a minimum shear stress must be exceeded to break the PS droplets, the role of screw speed was crucial. Therefore, for mixing/dispersion purposes, configuration 1 is

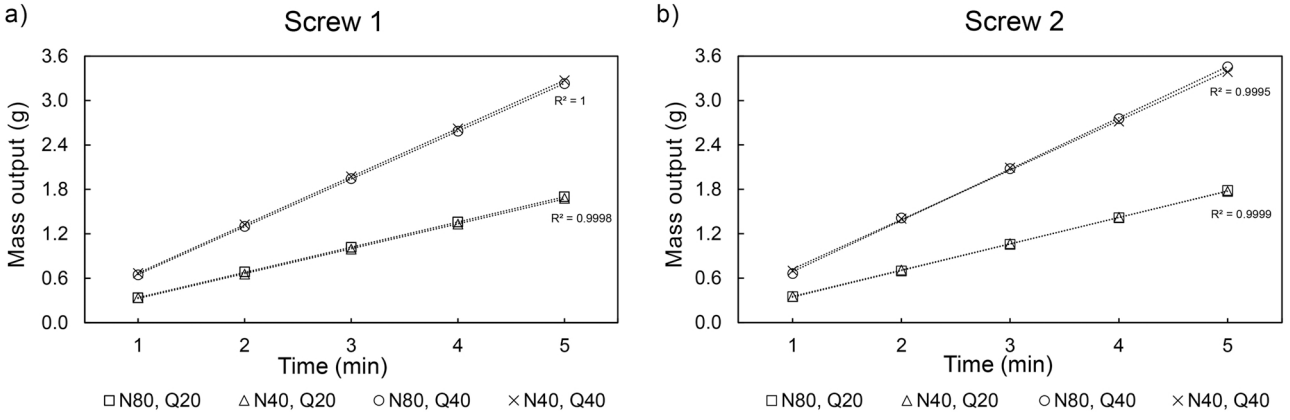

Fig. 7. Mass output at different screw rotation speeds and feed rates for (a) configuration 1 and (b) configuration 2.

Fig. 8. Screw pull-out experiments evidencing the influence of the screw configuration on the melting location: (a) configuration 1; (b) configuration 2.

Table 4
Influence of operating conditions on the residence times in the extruder.

Screw configuration	Screw speed (rpm)	Feed rate (g/h)	Minimum residence time (s)
1	40	20	355
		40	265
	80	20	264
		40	198
2	40	20	256
		40	197
	80	20	189
		40	139

better. Without the restrictive elements, processing with configuration 2 not only shifts melting downstream the screws, but also fails to induce the flow forces necessary to disperse the second phase component. The configuration 2, however, can be used when dispersion is not critical. Besides its low mixing capacity, the minimum residence times achieved with screw 2 are generally smaller, which can be positive when processing heat and/or shear sensitive materials.

Overall, the results from the extrusion tests demonstrate that the Co-TSE print head is potentially much more versatile than similar-sized single screw extrusion units developed for 3D printing. Thanks to the starve-feeding regime and screw modularity, its output is decoupled from the screw speed, and the effective screw length, residence times and mixing intensity can be tailored according to the intended application.

Besides, as widely recognized in the extrusion-related literature, the co-rotating twin screw extrusion offers much better mixing performance than equivalent single screw extruders (with similar diameter and length, operating in analogous conditions). As discussed, this is mostly attributed to the elongational flows created in the kneading zones, which are difficult to be achieved even with specialized mixing sections in single screws extruders [20,25].

5.2. 3D printing tests

Deposition tests were performed to determine the feasible speed range of the build platform (v_b) and characterize the uncompressed geometry of the beads. A simple G-code routine for line depositions was created and executed under various speeds with the extrusion output at 20 g/h. Screw configuration 1 was used, operating at 80 rpm. For better adhesion, the build platform was covered with PP adhesive tape and heated to 80 °C. The nozzle was kept 1 mm above the printing surface to avoid contact with the deposited beads. The resulting line depositions are shown in Fig. 11.

As expected, for a given extrusion output the lines become progressively narrower due to the stretching of the melt. Under the conditions tested, 3D printing can be considered feasible for deposition speeds up to 45 mm/s. After that, excessive stretching and the eventual rupture of the beads can occur. The width of the beads was measured at multiple points using the ImageJ software, and the height was measured using an analog micrometer. The influence of the valid deposition speeds on the bead geometry is shown in Fig. 12.

3D printing is possible in the whole range of depositions speeds, as long as the printing conditions are adjusted to the measured bead width and height. For example, printing at lower speeds requires setting larger line widths, in contrast to the narrower beads obtained at higher speeds. Nonetheless, the measurements show that the deposition is steadier in the range 20–40 mm/s. Outside that range, the printing parameters should be set to compensate for the observed variability, e.g. by increasing the overlapping between adjacent beads to avoid unfilled regions.

The data obtained from the line deposition tests were used to set up the 3D printing parameters for two type V tensile test specimens (ASTM D638) with 90/45° and 90° raster angle, respectively, a square scaffold, and a rectangular box with a spiralized contour (vase mode). The tensile specimens and scaffold were printed with screw 1, while the box was printed with screw 2. In all cases, the screw speed and feed rate were kept at 80 rpm and 20 g/h, respectively. The platform speed was set to 20 mm/s for all parts, with the exception of the walls of the box, which were printed at 15 mm/s. All parts were printed with a line width set to 0.8 mm. The layer height was 0.6 mm for the tensile specimens, and 0.4 mm for the scaffold and box. During printing of the latter, a few particles of red and yellow PP masterbatches were added to the PP at different times, to obtain a multicolored pattern, and to demonstrate the mixing capability of the extruder. The printed parts (Fig. 13) exhibited the quality expected from this 3D printing technique.

As shown in Fig. 12, for the 20 g/h output and using a 0.6 mm diameter nozzle, the width and height of the lines deposited at 45 mm/s can reach 0.49 ± 0.11 mm and 0.66 ± 0.05 mm, respectively. Similar to any other MEX system, the geometry of the deposited lines (i.e. bead

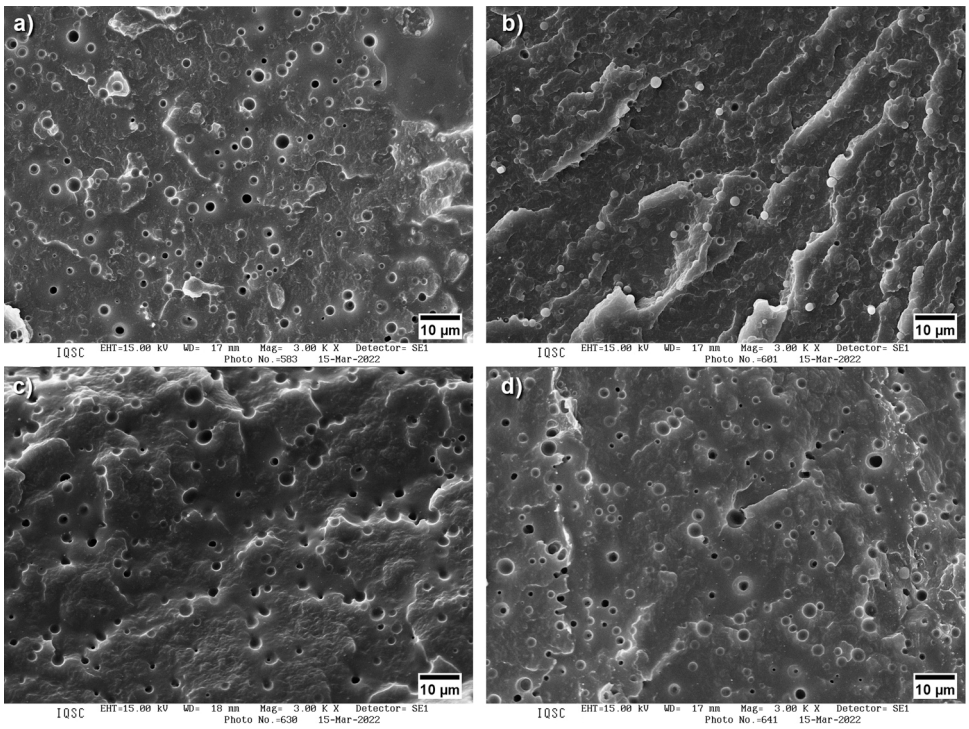

Fig. 9. Morphology of PP/PS 90/10 blends obtained by different processing conditions: a) screw 1, 40 rpm; b) screw 1, 80 rpm; c) screw 2, 40 rpm; d) screw 2, 80 rpm.

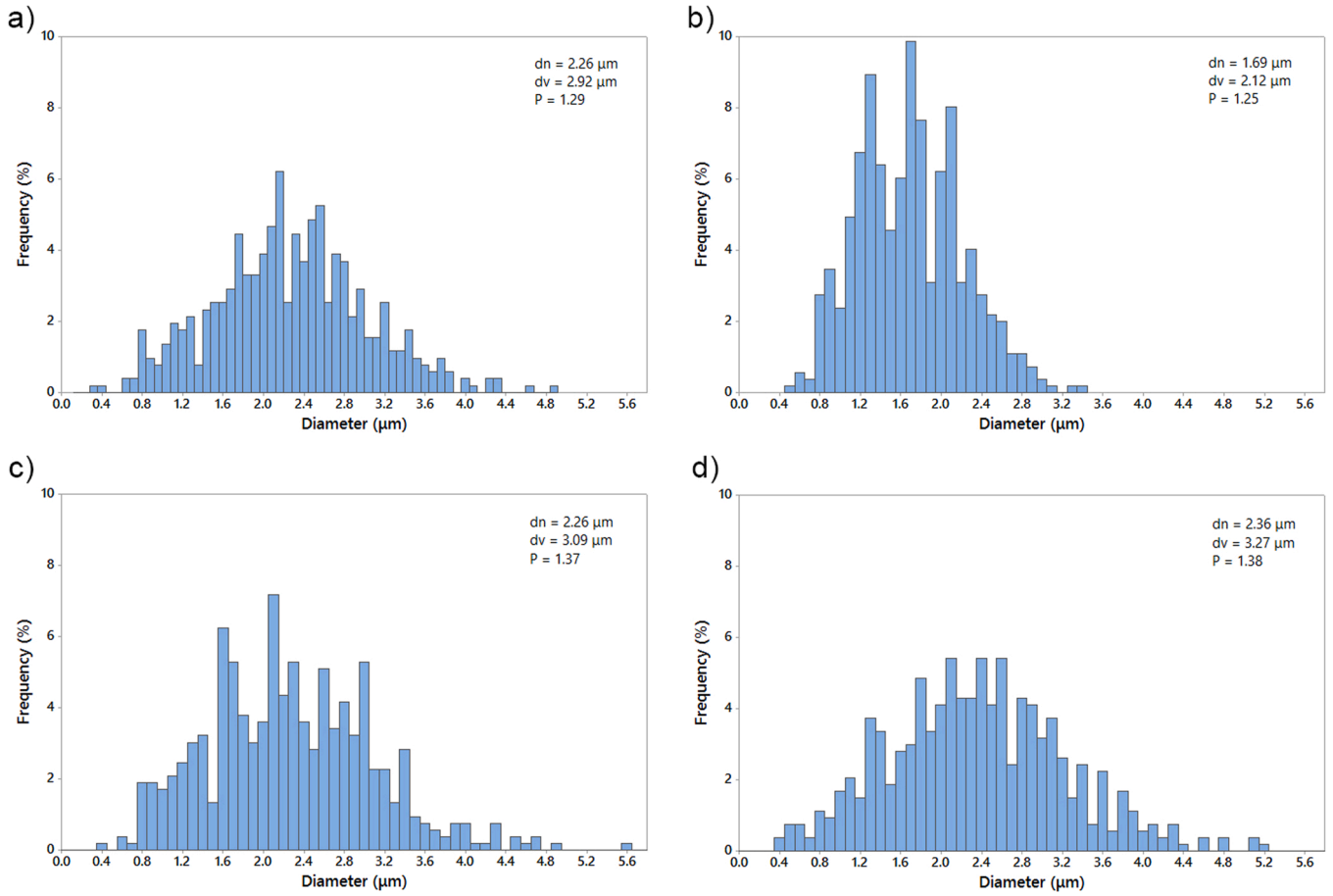

Fig. 10. Histograms of the PS droplet diameters in the PP/PS 90/10 blends processed with a) screw 1 at 40 rpm, b) screw 1 at 80 rpm, c) screw 2 at 40 rpm, and d) screw 2 at 80 rpm.

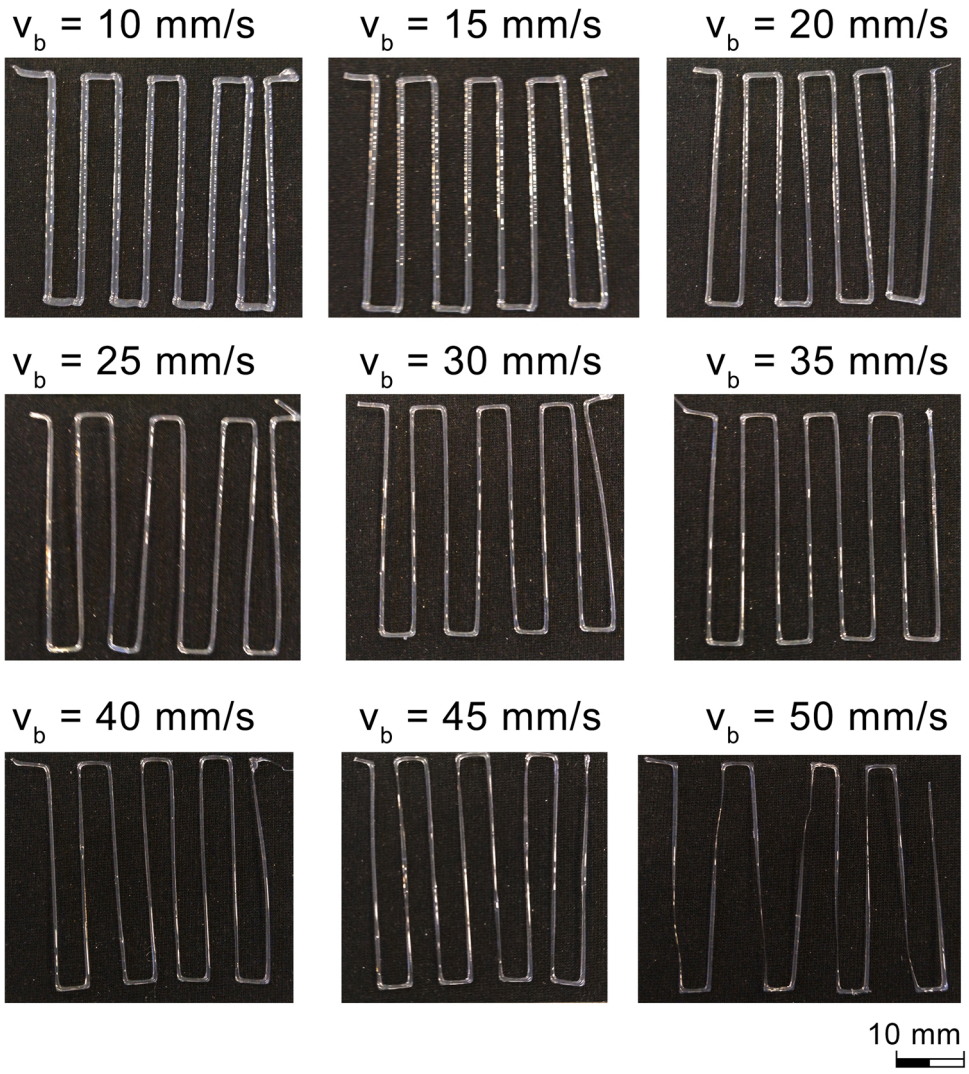

Fig. 11. Line depositions obtained at different build platform speeds, with 20 g/h output, 80 rpm, screw configuration 1.

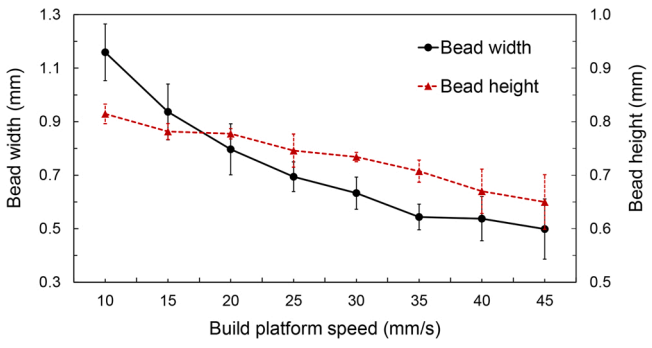

Fig. 12. Influence of build platform speed on the width and height of the deposited lines.

width and height) results from the interplay between output and printing parameters (e.g. build platform speed, nozzle diameter, and standoff distance). Therefore, by changing the nozzle diameter, finer strands can be obtained. This is demonstrated in Fig. 14, which compares the diameter of the extruded filament and the aspect of a scaffold generated with a 0.6 mm nozzle (same as in Fig. 13), and a 0.4 mm nozzle. The scaffold shown in Fig. 14b was printed with 0.4 mm raster width and 0.2 mm layer height, at 65 mm/s and 20 g/h output.

Uniaxial type V tensile specimens (with 90° raster angle) were 3D printed from the PP/PS 90/10 blend and the neat PP micro-pellets, using screw configuration 1 at 80 rpm and 20 g/h output (see Fig. 15). The barrel temperature was set to 180 °C and 210 °C for the first and second heating zones, respectively. The specimens were printed in the YX orientation (ASTM F2971–13). A 0.6 mm nozzle was used to print at 20 mm/s with 0.8 mm raster width, and 0.6 mm layer height (100 % infill).

Tensile tests were performed on an Instron 5969 universal testing machine, with an initial gauge length of 30 mm, at 10 mm/min and room temperature (25 °C). The measured values for the Young's modulus, ultimate tensile strength (UTS), and elongation at break are depicted in Fig. 16.

The values measured for the modulus and strength of the neat PP specimens (1179 ± 163 MPa and 25 ± 2 MPa, respectively) agree well with those reported by Carneiro et al. [28], who evaluated the mechanical properties of PP bars prepared by FDM. The PP specimens have also shown considerable ductility (100 ± 10 % elongation at break). As expected, the blend specimens showed an increase in the Young's modulus and UTS (1417 ± 101 MPa and 32 ± 1 MPa, respectively), accompanied by a significant decrease in the elongation at break (23 ± 6 %) due to the presence of the PS phase.

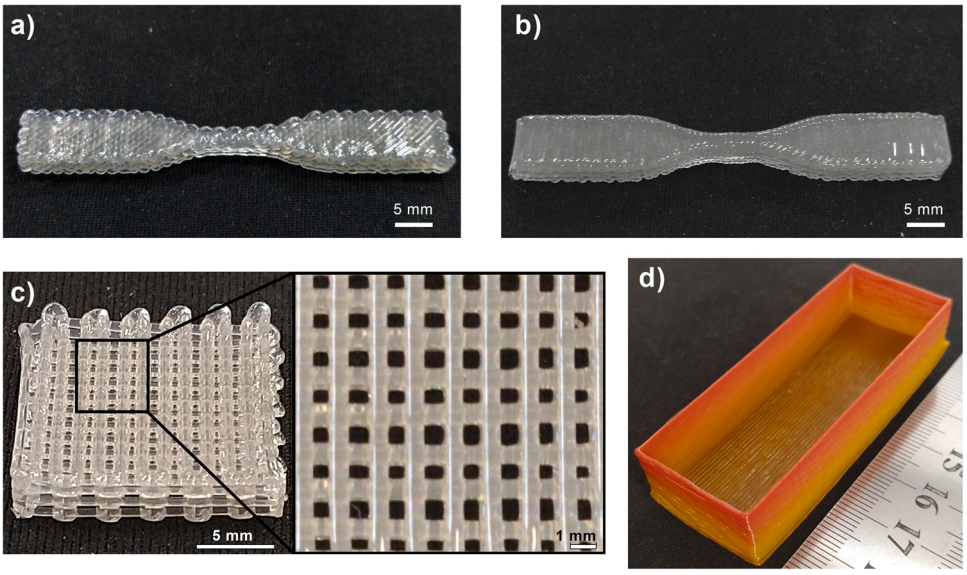

Fig. 13. 3D printed PP structures: (a) 90°/45° tensile specimen, (b) 90° tensile specimen, c) scaffold, d) box with a colored pattern.

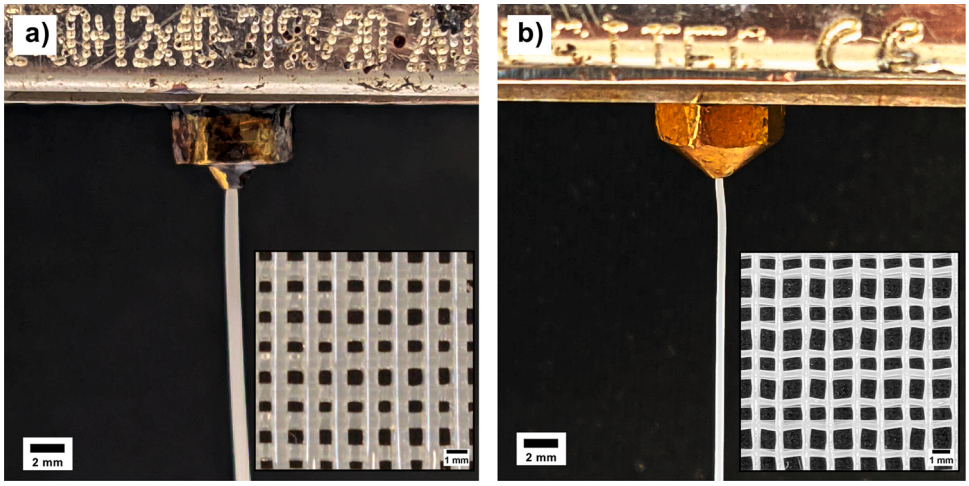

Fig. 14. Comparison of the extrudate diameter and achievable strand fineness with a a) 0.6 mm nozzle and b) a 0.4 mm nozzle.

6. Conclusions

A benchtop material extrusion additive manufacturing equipment based on a co-rotating twin screw extruder is designed and validated. It comprises three major subsystems: the extrusion unit, the drive unit, and the positioning system. The extrusion unit was designed with modular construction for improved geometrical flexibility. It includes a volumetric feeder that enables better control over the thermomechanical environment inside the extruder and reduces the required mechanical power. The design of the drive unit was particularly challenging, given the short distance between the screw shafts. The positioning system is responsible for the motion in the three Cartesian axes, a robust configuration considering the dimensions and inertia of the print head. With the presented embodiment, processing and printing can be performed with up to 75 cm^3 of powdered material, without the need to refill the feeder, and the maximum build is 55 × 80 × 43 mm.

Extrusion tests demonstrated that the Co-TSE print head is able to accept materials in powder or micro-pellet form, plasticize and extrude them through the nozzle under steady and controllable flow rate. Since the output and the screw speed are controlled independently, distributive and dispersive mixing intensity and residence time can be varied without affecting the extrusion/deposition rate. Two screw configurations were used, with and without kneading discs, to assess the response of the extrusion unit in terms of flow characteristics and mixing performance. The screw with kneading elements (configuration 1) is particularly effective for mixing/dispersion purposes. In addition, based on the literature, the mixing performance offered by the Co-TSE is expected to be superior to what is achievable with similar-sized single screw extruders developed for 3D printing.

Deposition tests were performed to find the feasible printing conditions, including the deposition speed, beads width, and layer height. Since the screw profile and speed did not affect the output, the extrusion conditions were not varied thoroughly. The resulting insights from the initial single layer depositions were used to set the printing conditions for more complex parts. Tensile test specimens, a square scaffold, and a rectangular box with multicolored walls were printed with the expected quality, demonstrating the global feasibility of the design. The specimens were pulled, showing good agreement with the expected results.

The Co-TSE AM system not only eliminates the dependency on filamentary feedstock but combines polymer compounding and 3D printing in a single processing route. This represents a significant step towards the availability of a more versatile equipment that can be customized according to the required processing tasks and/or intended application. Future research avenues include using this printer to integrate into a

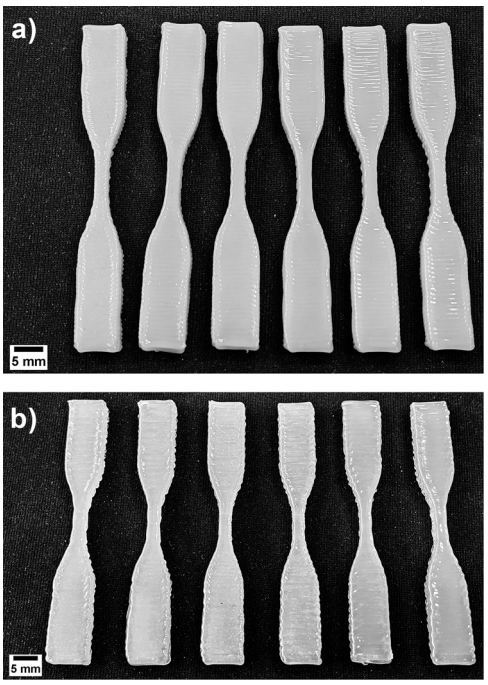

Fig. 15. 3D printed tensile test specimens from a) PP/PS 90/10 blend and b) neat PP.

single step the manufacture and printing of polymer blends, bio-composites, and bio-nanocomposites for personalized medical applications.

Funding information

This work was supported by the National Council for Scientific and Technological Development (CNPq), grants 2016-4/442109 and 142348/2018-0, and by the Coordination for the Improvement of Higher Education Personnel (CAPES), finance code 001.

Ethics approval

The work contains no libelous or unlawful statements, does not infringe on the rights of others, or contains material or instructions that might cause harm or injury.

CRediT authorship contribution statement

Alessandra de Almeida Lucas: Supervision, Funding acquisition. **Marcelo Aparecido Chinelatto:** Writing – review & editing, Supervision, Methodology, Conceptualization. **Amir Ilkiu Sarout:** Investigation. **Andre Luiz Grando Santos:** Investigation. **António Gaspar-Cunha:** Supervision, Investigation. **José António Covas:** Writing – review & editing, Writing – original draft, Supervision, Methodology. **Jorge Lino Alves:** Writing – review & editing, Supervision. **Joaquim Manoel Justino Netto:** Writing – review & editing, Writing – original draft, Visualization, Methodology, Investigation, Data curation, Conceptualization. **Zilda de Castro Silveira:** Writing – review & editing, Writing – original draft, Supervision, Project administration, Methodology, Funding acquisition, Conceptualization.

Declaration of Competing Interest

The authors declare the following financial interests/personal relationships which may be considered as potential competing interests: Joaquim Manoel Justino Netto has patent #BR 10 2017 022948 3 pending to University of Sao Paulo.

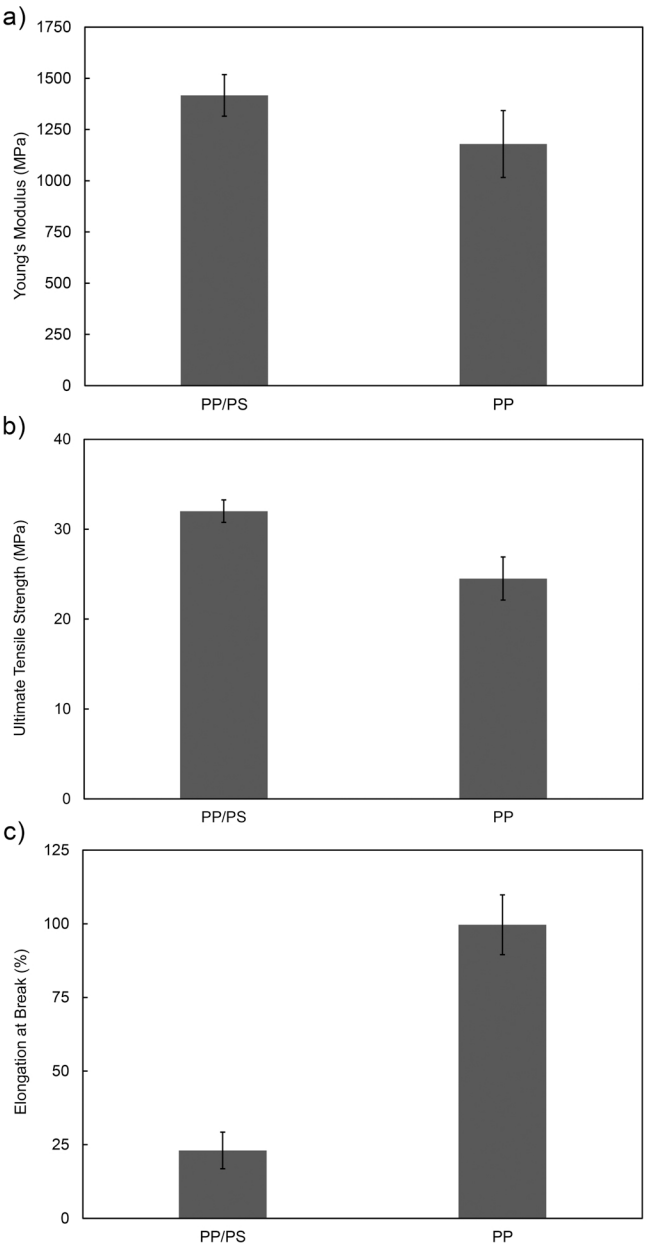

Fig. 16. Tensile testing results for PP/PS and PP: a) Young's modulus, b) ultimate tensile strength, and c) elongation at break.

Data Availability

Data will be made available on request.

Acknowledgements

The authors would like to thank Dr. André L. J. Munhoz, researcher at the Instituto Nacional de C&T em Biofabricação - Unicamp, Brazil, and Dr. Julian Ávila, professor at the Faculdade de Engenharia Eletrônica e de Telecomunicações e Engenharia Aeronáutica - UNESP, Brasil, for the assistance in manufacturing the rigid couplings.

Data Availability

Not applicable.

Consent to participate

The authors consent to participate.

Consent for publication

The authors consent to publish.

References

[1] S.S. Crump, Apparatus and method for creating three-dimensional objects, US patent 5121329A, 1992.

[2] I. Gibson, D. Rosen, B. Stucker, M. Khorasani, Additive Manufacturing Technologies, 3rd ed., Springer Nature: Switzerland, 2021.

[3] M. Leary, Design for Additive Manufacturing, 1st ed., Elsevier, Amsterdam, The Netherlands, Chap. 1, pp. 1–6, 2020. ⟨https://doi.org/10.1016/B978-0-12-816721-2.00001-4⟩.

[4] C. Teixeira, A. Gaspar-Cunha, J.A. Covas, Flow and heat transfer along the length of a co-rotating twin screw extruder, Polym.-Plast. Technol. Eng. 51 (15) (2012) 1567–1577, https://doi.org/10.1080/03602559.2012.716477.

[5] J.M. Justino Netto, H.T. Idogava, L.E. Frezzatto Santos, Z.C. Silveira, P. Romio, J. L. Alves, Screw-assisted 3D printing with granulated materials: a systematic review, Int. J. Adv. Manuf. Technol. 115 (2021) 2711–2727, https://doi.org/10.1007/s00170-021-07365-z.

[6] D.J. Byard, A.L. Woern, R.B. Oakley, M.J. Fiedler, S.L. Snabes, J.M. Pearce, Green fab lab applications of large-area waste polymer-based additive manufacturing, Addit. Manuf. 27 (2019) 515–525, https://doi.org/10.1016/j.addma.2019.03.006.

[7] M.J. Reich, A.L. Woern, N.G. Tanikella, J.M. Pearce, Mechanical properties and applications of recycled polycarbonate particle material extrusion-based additive manufacturing, Materials 12 (10) (2019) 1642, https://doi.org/10.3390/ma12101642.

[8] C. Wang, L. Zhang, Y. Fang, W. Sun, Design, characterization, and 3D printing of cardiovascular stents with zero poisson's ratio in longitudinal deformation, Engineering 7 (7) (2020) 979–990, https://doi.org/10.1016/j.eng.2020.02.013.

[9] A. Wibowo, C. Vyas, G. Cooper, F. Qulub, R. Suratman, 3D Printing of polycaprolactone–polyaniline electroactive scaffolds for bone tissue engineering, Materials 13 (3) (2020) 512, https://doi.org/10.3390/ma13030512.

[10] B. Huang, C. Vyas, J.J. Byun, M. El-Newehy, Z. Huang, P. Bartolo, Aligned multi-walled carbon nanotubes with nanohydroxyapatite in a 3D printed polycaprolactone scaffold stimulates osteogenic differentiation, Mater. Sci. Eng. C 108 (2020), 110374, https://doi.org/10.1016/j.msec.2019.1103744.

[11] J. Tian, R. Zhang, J. Yang, W. Chou, P. Xue, Y. Ding, Additive manufacturing of wood flour/PHA composites using micro-screw extrusion: effect of device and process parameters on performance, Polymers 13 (7) (2021) 1107, https://doi.org/10.3390/polym13071107.

[12] C. Vyas, J. Zhang, Ø. Øvrebø, B. Huang, I. Roberts, M. Setty, B. Allardyce, H. Haugen, R. Rajkhowa, P. Bartolo, 3D printing of silk microparticle reinforced polycaprolactone scaffolds for tissue engineering applications, Mater. Sci. Eng. C 118 (2021), 111433, https://doi.org/10.1016/j.msec.2020.111433.

[13] W. Lengauer, I. Duretek, M. Furst, V. Schwarz, J. Gonzalez-Gutierrez, S. Schuschnigg, C. Kukla, M. Kitzmantel, E. Neubauer, C. Lieberwirth, V. Morrison, Fabrication and properties of extrusion-based 3Dprinted hardmetal and cermet components, Int. J. Refract Met. Hard Mater. 82 (2019) 141–149, https://doi.org/10.1016/j.ijrmhm.2019.04.011.

[14] H. Kim, S. Lee, Printability and physical properties of iron slag powder composites using material extrusion-based 3D printing, J. Iron Steel Res. Int. 28 (2020) 111–121, https://doi.org/10.1007/s42243-020-00475-0.

[15] G. Singh, J.M. Missiaen, D. Bouvard, J.M. Chaix, Additive manufacturing of 17–4 PH steel using metal injection molding feedstock: analysis of 3D extrusion printing, debinding and sintering, Addit. Manuf. 47 (2021), 102287, https://doi.org/10.1016/j.addma.2021.102287.

[16] Q. He, J. Jiang, X. Yang, L. Zhang, Z. Zhou, Y. Zhong, Z. Shen, Additive manufacturing of dense zirconia ceramics by fused deposition modeling via screw extrusion, J. Eur. Ceram. Soc. 41 (1) (2021) 1033–1040, https://doi.org/10.1016/j.jeurceramsoc.2020.09.018.

[17] A. Goyanes, N. Allahham, S.J. Trenfield, E. Stoyanov, S. Gaisford, A.W. Basit, Direct powder extrusion 3D printing: fabrication of drug products using a novel single-step process, Int. J. Pharm. 567 (2019), 118471, https://doi.org/10.1016/j.ijpharm.2019.118471.

[18] J.J. Ong, A. Awad, A. Martorana, S. Gaisford, E. Stoyanov, A.W. Basit, A. Goyanes, 3D printed opioid medicines with alcohol-resistant and abuse-deterrent properties, Int. J. Pharm. 579 (2020), 119169, https://doi.org/10.1016/j.ijpharm.2020.119169.

[19] A. Samaro, B. Shaqour, N.M. Goudarzi, M. Ghijs, L. Cardon, M.N. Boone, B. Verleije, K. Beyers, V. Vanhoorne, P. Cos, C. Vervaet, Can filaments, pellets and powder be used as feedstock to produce highly drug-loaded ethylene-vinyl acetate 3D printed tablets using extrusion-based additive manufacturing, Int. J. Pharm. 607 (2021), 120922, https://doi.org/10.1016/j.ijpharm.2021.120922.

[20] C. Rauwendaal. Polymer Extrusion, 5th ed., Carl Hanser Verlag, Munich, Germany, 2014.

[21] A. Bhattacharyya, G. Janarthanan, H.N. Tran, H.J. Ham, J.H. Yoon, I. Noh, Bioink homogeneity control during 3D bioprinting of multicomponent micro/nanocomposite hydrogel for even tissue regeneration using novel twin screw extrusion system, Chem. Eng. J. 415 (2021), 128971, https://doi.org/10.1016/j.cej.2021.128971.

[22] H. Bai, W. Qin, S. Jia, L. Ren, Y. An, J. Bao, A new type of 3D printing molding equipment: overall structural design and the numerical simulation for the flow field characteristics of its screw module, Int. J. Precis. Eng. Manuf. 22 (2021) 1639–1656, https://doi.org/10.1007/s12541-021-00564-4.

[23] J.M. Justino Netto, Z.C. Silveira, Design of an innovative three-dimensional print head based on twin-screw extrusion, J. Mech. Des. 140 (12) (2018), 125002, https://doi.org/10.1115/1.4041175.

[24] P.H.M. Elemans, Polymer Twin-Screw Extrusion: Melting, Mixing and Screw Design", Reference Module in Materials Science and Materials Engineering, Elsevier, 2016, ISBN 9780128035818. ⟨https://doi.org/10.1016/B978-0-12-803581-8.03364-6⟩.

[25] K. Kohlgrüber, Co-Rotating Twin-Screw Extruders, Carl Hanser Verlag, Munich, Germany, 2008.

[26] O.S. Carneiro, J.A. Covas, J.A. Ferreira, M.F. Cerqueira, On-line monitoring of the residence time distribution along a kneading block of a twin-screw extruder, Polym. Test. 23 (2004) 925–937, https://doi.org/10.1016/j.polymertesting.2004.05.001.

[27] L.B. Canto, On the coarsening of the phase morphology of PP/EVA blends during compounding in a twin screw extruder, Polym. Test. 34 (2014) 175–182, https://doi.org/10.1016/j.polymertesting.2014.01.012.

[28] O.S. Carneiro, A.F. Silva, R. Gomes, Fused deposition modeling with polypropylene, Mater. Des. 83 (2015) 768–776, https://doi.org/10.1016/j.matdes.2015.06.053.